

# INFLUENCE OF LUBRICANT TEMPERATURE, LUBRICANT LEVEL AND ROTATIONAL SPEED ON THE CHURNING POWER LOSS IN AN INDUSTRIAL PLANETARY SPEED REDUCER: COMPUTATIONAL AND EXPERIMENTAL STUDY

FRANCO CONCLI & CARLO GORLA

Politecnico di Milano, Mechanical Department, Milan, Italy.

## ABSTRACT

Planetary speed reducers are applied in a wide range of applications. Their main advantages are the compact design and high power density. For this reason, the demand for high efficiency gearboxes is continuously increasing and this is also why models to predict the additional churning loss, characteristic of this kind of gearing, are required. The particular configuration of the planetary speed reducers, in fact, entails an additional motion with a circular path around the gearbox axis of the planetary gears due to the rotation of the planet carrier on which they are mounted and this induces an additional source of loss. Having efficiency prediction models allows, in fact, comparison of different solutions during the design step. Literature provides some prediction models for ordinary gears but no models are still available for planetary gears. This report introduces a computational and experimental analysis of this kind of loss. Many simulations have been performed and the influence of many operating conditions like lubricant level and temperature and the rotational speed of the planet carrier have been studied. Moreover, the results of an experimental testing campaign on a specially designed gearbox are presented and compared with the computational ones to validate the model. The two approaches give results in good agreement.

*Keywords:* Churning loss, efficiency, multiphase flow simulation, planetary speed reducers, volume of fluid.

## 1 INTRODUCTION

Efficiency improvement is the new challenge in all fields of design. In this scenario, the reduction of power loss is becoming more and more a main concern also in the design of power transmissions. For this reason, it is important to have some models to quantify the power loss since the design stage.

The power loss of a mechanical transmission can be subdivided primarily into bearing loss, seal loss, meshing loss and churning loss. Literature provides some models for the prediction of all kinds of loss [1–4]. What is still missing is an appropriate model for the prediction of the additional churning loss characteristic of the planetary gears. In this kind of gearing, in fact, the motion of the planetary gears due to the planet carrier rotation induces an additional source of loss. For this reason the authors are studying in depth this phenomena [5, 6–10].

The aim of this study is to provide a model for the correct estimation of this kind of loss and, consequently, for the correct estimation of the efficiency of the whole transmission.

By means of numerical simulations, the influence of some parameters like lubricant level, lubricant temperature, and rotational speed of the planet carrier have been studied. The model has been carried out by means of a Volume of Fluid (VOF) analysis on a commercial code and simulates the behaviour of the air–oil lubricant mixture in the whole casing.

To validate the computational results, some experiments have been carried out on a specially modified speed reducers. The computational and the measured results are in good agreement.

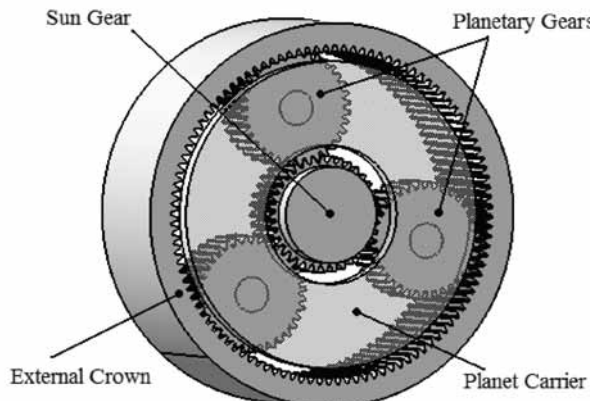


Figure 1: Planetary gearing.

## 2 PROBLEM DEFINITION

A typical configuration of a planetary gearing is shown in Fig. 1: the sun gear, the planetary gears, the planet carrier and the external crown can be seen.

To use a planetary gearing, it is necessary to remove a degree of freedom. The most adopted solution is to fix the external crown to the ground. With this solution the power flows from the sun gear shaft to the planet carrier shaft through the planetary gears: this fact implies that the planetary gear motion is made of two components: the first one is a rotation of the gears around their axis and the second one is a motion with a circular path around the gearbox axis due to the planet carrier rotation on which they are mounted.

The speed reducers are generally oil splash lubricated, and it is just the interaction between the rotating elements and the lubricant air–oil mixture, which is the source of churning loss. In planetary gearing, as described above, the planetary gears have not only the rotation around their axis but also the motion with a circular path together with the planet carrier. The multiphase fluid dynamics of the lubricant is the subject of this study.

The most influencing parameters are the oil level and its properties, such as the viscosity and the density (functions of the temperature), the geometry and, of course, the rotational speed. The transmitted torque influences this kind of loss indirectly: increasing the transmitted torque means more load dependent power loss (like the meshing ones and part of the bearing ones) and, consequently, a higher regime temperature of the lubricant.

## 3 GEOMETRY MODIFICATIONS

In this research, the behaviour of a real planetary speed reducer provided by Tecnoingranaggi® has been simulated. It is a MP.IS.105.1.4.15 industrial speed reducer (Fig. 2) characterized by a sun gear connected to the input shaft, three planetary gears and a ‘double disk’ planet carrier connected to the output shaft. Both, the input and the output shaft, are mounted by means of two bearings (model SKF 6205 and 6207, respectively). Two contact seal are also present to avoid leakage of lubricant. To evaluate the churning power loss related to the motion of the planetary gears around the gearbox axis due to the rotation of the planet carrier, the original geometry of the speed reducer has been modified. The teeth of the external crown have been removed by machining and the sun gear has been substituted with a smaller and cylindrical (without teeth) component. The aim of this modifications is to prevent

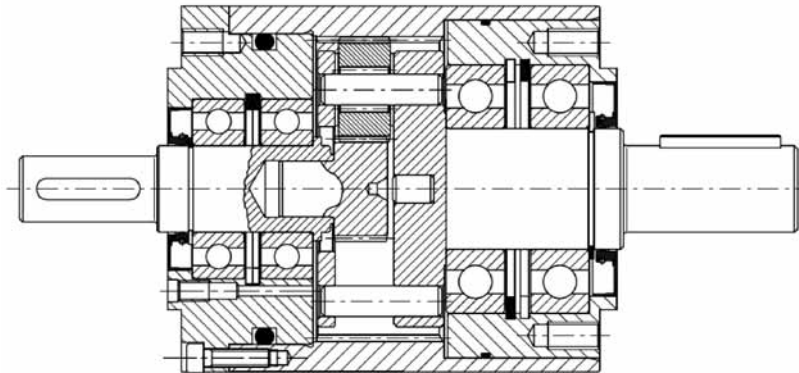


Figure 2: Initial geometry of the speed reducer.

the engaging of the gears, avoiding sliding loss and churning loss due to the rotation of the gears around their axis. This modified geometry has been used both for the numerical simulations and the experimental testing campaign.

On the other hand, these modifications also eliminate the churning loss due to the rotation of the planets around their axis. These kind of losses have been already studied and the ISO standards [3] provide some models to predict them. Quantitatively this losses are some order of magnitude lower in comparison with the churning loss caused by the rotation of the planet carrier and the planets around the gearbox axis.

#### 4 SIMULATION SETUP

The first part of the research was to build a model for the numerical simulations.

##### 4.1 Geometry and mesh

The domain for the CFD analysis is the internal free volume of the speed reducer after the above-described geometry modifications. Figure 3 shows this volume marked in grey.

The computational domain for the CFD analysis has been modelled by means of a 3D CAD software and discretized with a swept mesh. This meshing technique consists in creating a mesh on one side of the region, known as the source side, and then copying the nodes of that mesh, one element layer at a time, until the final side, known as the target side, is reached.

Different meshes have been tested. The final model has been discretized with about 500,000 hexahedral cells. This kind of elements allows a larger aspect ratio compared with the tetrahedral cells in which it will invariably affects the skewness of the cell, which is undesirable as it may impede accuracy and convergence. Some trials with finer (1E6) and coarser (1E5) meshes have been performed. Finally, the number of 500,000 cells has been chosen as the best one, because it conjugate good results and computational times avoiding convergence problems.

##### 4.2 Parameter setting

To simulate the lubricant behaviour, the VOF multiphase approach of the commercial code Fluent has been used. The VOF formulation relies on the fact that two or more fluids

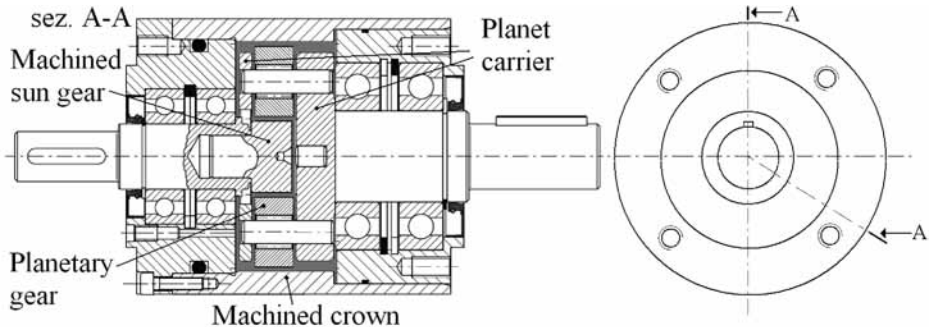


Figure 3: Modified geometry of the speed reducer: the computational domain is marked in grey.

(or phases) are not inter-penetrating. The fields for all variables and properties are shared by the phases and represent volume-averaged values, as long as the volume fraction of each of the phases is known at each location. Thus, the variables and properties in any given cell are either purely representative of one of the phases, or representative of a mixture of the phases, depending upon the volume fraction values. The tracking of the interface between the phases is accomplished by the solution of a continuity equation for the volume fraction of one of the phases

$$\frac{\partial}{\partial t} (a_q \rho_q) + \nabla \cdot (a_q \rho_q \vec{v}_q) = S_{a_q} + \sum_{p=1}^n (\dot{m}_{pq} - \dot{m}_{qp}) \quad (1)$$

where  $\rho_q$  is the density of the  $q^{th}$  phase,  $a_q$  the volume fraction of that phase,  $\dot{m}_{pq}$  and  $\dot{m}_{qp}$  the mass transfer from phase  $q$  to phase  $p$  and vice versa, respectively, and  $S_{a_q}$  the source term, in this case equal to zero. This volume fraction equation has been solved by means of an explicit scheme discretization to avoid the numerical diffusion. Which means solving

$$\frac{a_q^{n+1} \rho_q^{n+1} - a_q^n \rho_q^n}{\Delta t} V + \sum_f (\rho_q^n U_f^n a_{q,f}^n) = \left[ S_{a_q} + \sum_{p=1}^n (\dot{m}_{pq} - \dot{m}_{qp}) \right] V \quad (2)$$

where  $n+1$  and  $n$  are the indexes for the new time step and the previous one,  $a_{q,f}^n$  is the face value of the  $q^{th}$  volume fraction computed with the Geo-Reconstruction scheme,  $V$  is the volume of the cell  $U_f^n$  and is the volume flux on the face. The Geo-Reconstruction approach is an accurate scheme which assumes that the interface between two fluids has a linear slope within each cell, and uses this linear shape for the calculation of the advection of fluid through the cell faces. This scheme avoids the numerical diffusion but needs an accurate grid.

The properties appearing in the above transport equations are determined by the presence of the component phases in each control volume. In a two-phase system, if the phases are represented, for example, by the subscripts air and oil, and if the volume fraction of the second of these is being tracked, then the density in each cell is given by

$$\rho = \rho_{oil} a_{oil} - \rho_{air} (1 - a_{oil}) \quad (3)$$

Table 1: Properties of the two phases at 40°C.

	$\rho$ 40°C [Kg/m3]	$\nu$ 40°C [Kg/ms]
Air	1.225	1.7894E-05
Lubricant oil	1041	0.2082

All other properties are calculated in the same manner.

The two phase properties are summarized in Table 1.

The oil used in the simulations is the same oil actually used for the lubrication of this kind of speed reducers. It is a Klübersynth GH 6–220 oil.

Under the operating conditions options, as operating density has been chosen the lowest one, corresponding to the air density.

A single momentum equation is solved throughout the domain, and the resulting velocity field is shared among the phases

$$\frac{\partial}{\partial t}(\rho \vec{v}) + \nabla \cdot (\rho \vec{v} \vec{v}) = -\nabla p + \nabla \cdot [\mu (\nabla \vec{v} + \nabla \vec{v}^T)] + \rho \vec{g} + \vec{F} \quad (4)$$

One limitation of the shared-fields approximation is that in cases where large velocity differences exist between the phases, the accuracy of the velocities computed near the interface can be adversely affected. This is not the case: in the speed reducer, lubricant and air have the same global behaviour and approximately the same speeds.

For the pressure–velocity-coupling, a SIMPLE scheme has been adopted as suggested for the flows in closed domains [11,12]. This algorithm uses a relationship between velocity and pressure corrections to enforce mass conservation and to obtain the pressure field. For compressible flows, the unknown is the density and the pressure is evaluated with a constitutive equation. The solution of the system of equations for incompressible flows, in turn, is accomplished by the fact that there are no equations where the pressure is explicitly defined. To calculate it, the continuity equation is substituted with an equation for the pressure; with some manipulation, the pressure appears like unknown term in the momentum equation.

To reproduce the operating conditions of the speed reducer, a rigid motion of the mesh has been applied. The motion has been defined by means of an User defined Function (UdF) as a rigid rotation with a fixed rotational speed around the gearbox axis. With this mesh motion, it is possible to reproduce the real operating conditions in which the planet carrier together with the planets rotates around the gearbox axis.

The internal boundaries, corresponding to the planet carrier and planetary gear surfaces, rotate together with the mesh (marked in dark grey in the Fig. 4), while the other boundaries, corresponding to the external crown and the case of the gearbox (marked in black in the Fig. 4), are set like stationary in the absolute reference frame. Due to the geometry, it was also possible to solve the problem by creating two separate partitions and by imposing a mesh sliding between them. However, in that case, some additional equations have to be solved, to manage interactions between the cells at the sliding interface, and the computational time will therefore increase. For this reason the global mesh motion has been selected as the best solution. Both boundaries have been set to no slip walls.

The time step for the transient analysis has been chosen as dynamic. This means that every step, the new time increment depends on the velocity field.

$$\Delta t = \frac{V_{cell,min}^3}{U} \quad (5)$$

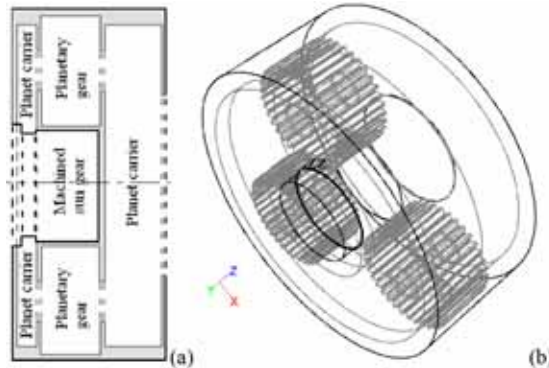


Figure 4: (a) Two-dimensional schematization of the computational domain (section A-A Fig. 3) and (b) 3D representation of the computational domain.

where  $V_{cell,min}$  is the volume of the smallest cell in the computational domain and  $U$  is the velocity scale of the problem. This allows the increase in the calculations without the risk of losing the convergence. The time step used for the volume fraction calculation is not the same of the time step used for the transport equations. The code solves the volume fraction equations once for each time step. This means that the convective flux coefficients appearing in the other transport equations for each iteration are not completely updated, since the volume fraction fields will not change from iteration to iteration. This choice was taken to have less computational time since the number of iteration at each time step is always lower than five and this approximation will not affect the results.

#### 4.3 Operating conditions

The purpose of the simulations is to calculate the power loss under different operating conditions.

To do that, the resistant torque on the planet carrier shaft has been monitored. This resistant torque is calculated with a surface integral on the moving walls with respect to the gearbox axis and it is composed of two parts: the first given by the pressure and the second by the viscous effects. The simulations have been computed with different combinations of oil level, operating temperature (which means different density and viscosity) and rotational speed.

Table 2 shows the combinations of parameters for each simulation.  $T$  is the operating temperature in degree Celsius,  $\omega$  the rotational speed of the planet carrier in rpm and  $L$  is the oil level in millimetre measured from the gearbox axis (positive if higher than the axis, negative if lower).

The analysis have been started from the stationary condition in which the lubricant lies at the bottom of the speed reducer (Fig. 5a). The analysis has been stopped after the resistant torque had no more sensible fluctuations and was stabilized. By multiplying the mean value of the torque by the imposed rotational speed, it is possible to determine the churning power loss.

Figure 5c–e shows the behaviour of the lubricant in the mid-section after the regime condition is reached. The lubricant is thrown away from the gearbox axis and it lies primarily on the external crown.

Table 2: Parameters for each simulation.

T [°C]	L[mm]	$\omega$ [rpm]
40	20	500
40	0	500
40	0	1500
40	20	1000
40	20	1500
40	0	1000
40	-20	500
40	-20	1000
40	-20	1500
20	0	1000
65	0	1000

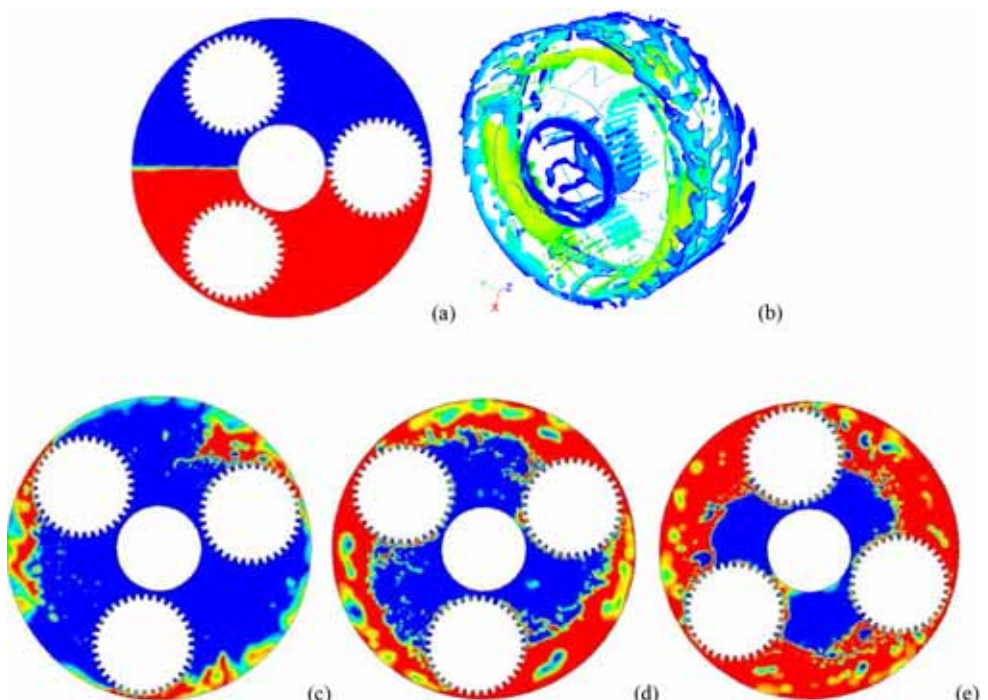


Figure 5: (a) Contours of volume fraction for the oil phase in the mid-section at the first time step; (b) contours of velocity magnitude for the oil phase in the whole domain ( $L = 0$  mm); (c) contours of volume fraction for the oil phase in the mid-section after the reach of the regime condition ( $L = -20$  mm); (d) contours of volume fraction for the oil phase in the mid-section after the reach of the regime condition ( $L = 0$  mm); (e) contours of volume fraction for the oil phase in the mid-section after the reach of the regime condition ( $L = 20$  mm).

## 5 EXPERIMENTAL TESTS

To provide a validation of the numerical model, the industrial planetary speed reducer has been physically modified as already described and tested. After the geometry modifications, the input shaft and the output shaft are completely uncoupled. That allows to move the planet carrier independently and to reproduce the condition in which the meshing loss and the churning loss due to the rotations of the gears around their axis are avoided.

A schematic layout of the test rig is shown in Fig. 6. The speed reducer is fixed to the ground by means of a specially designed structure. The planet carrier shaft is connected to a HBM T12 torque metre (Table 3) with a telemetric transmission of the signal by means of a double cardan. The torque metre, in turn, is connected to a 35KW DC motor by means of a coupling (Fig. 7).

A transparent pipe allows the monitoring of the actual oil level. The operating temperature can be imposed by a special heating system (insulated chamber with a heating source) and measured by means of a thermocouple. The rotational speed can be controlled by the motor programmable logic controller (PLC).

The power is transferred through the torque metre (where is measured) and then enters the speed reducers. In the speed reducer, this power is partially dissipated by the internal bearings (2 SKF 6207 bearing) and by its seal and partially is dissipated to move the lubricant (churning losses). All the power that enter the speed reducer is dissipated like heat.

For each of the three oil levels, four different temperatures have been tested. For all this coupled operating conditions (oil level + temperature) the power loss have been measured in a rotational speed range between 100 and 1500 rpm.

## 6 RESULTS

Before comparing the experimental results with the computated ones, it is necessary to subtract the seal loss and the bearing loss from the measured values. The torque metre, in fact, measures the input power of the reducer. A little fraction of this power is dissipated by the

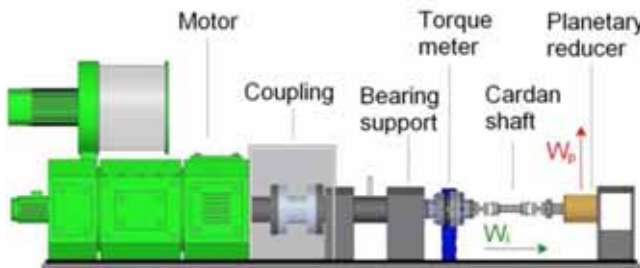


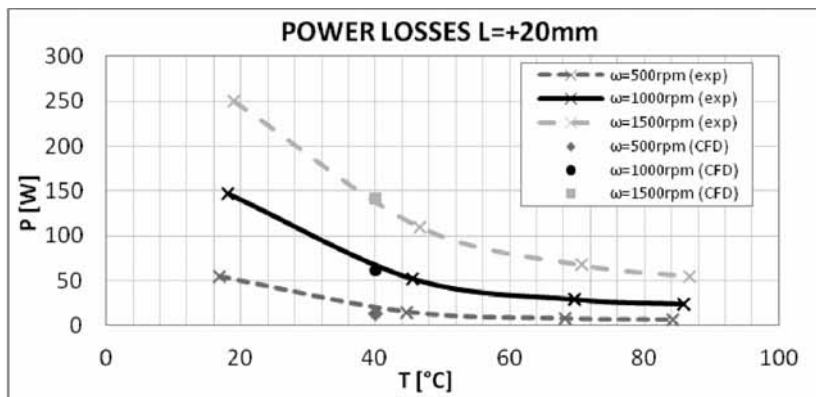
Figure 6: Schematic layout of the test rig.

Table 3: Specification of the instruments.

	Torque meter	Thermocouple
<b>Model</b>	HBM T12	MTS40161T150–2000+H
<b>Range</b>	0÷6000 Hz 0÷500 Nm	-200÷400°C
<b>Error</b>	0.01%FS	0.1°C



Figure 7: Test rig with the tested speed reducer.

Figure 8: Experimental and computation results for  $L = 20$  mm.

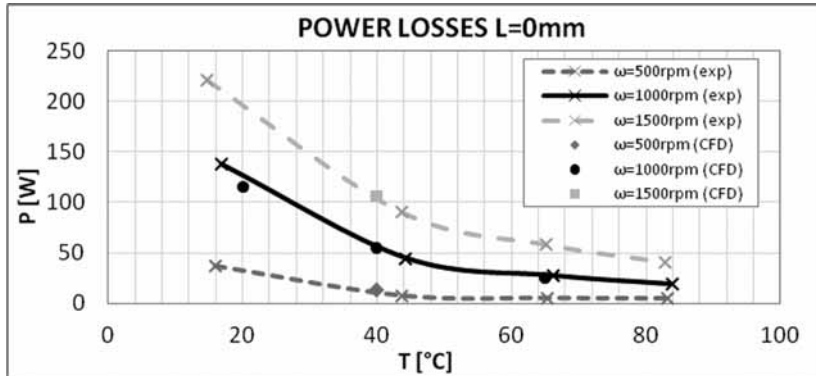
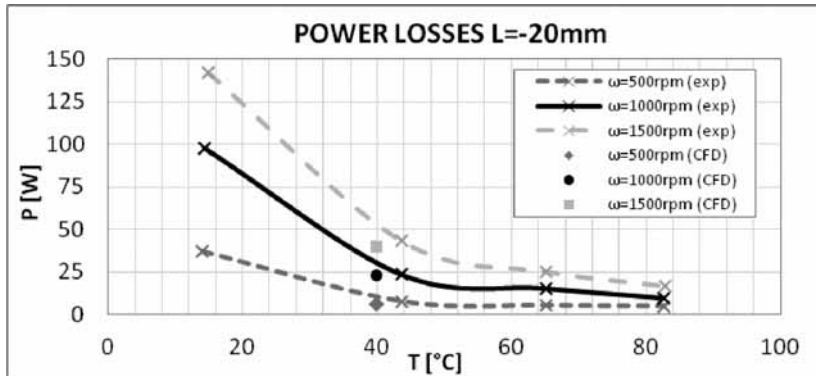
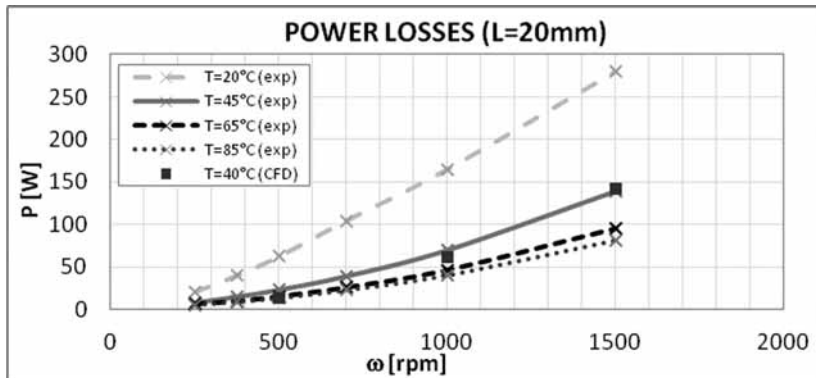
two internal bearings of the planet carrier shaft and by its seal. This part of loss can be easily calculated by means of some proved models [1,2] as function of the testing conditions.

To evaluate this loss, the SKF model has been adopted. Performing specific tests on the bearings, in fact, it is extremely complicated because to avoid the churning loss, the only way is to remove the planet carrier and the planets. However, this modification changes the lubrication condition of the bearings giving wrong results. A solution can be an additional torque metre mounted inside the speed reducer, between the bearings and the planet carrier.

At this point, the focus of the research was on the churning loss, so it has been chosen to use an empirical model to calculate the bearing losses, but this experimental tests will be of course performed in the future.

In the adopted model, the resistant torque is calculated like a sum of the rolling frictional moment  $M_{rr} = G_{rr}(vn)^{0.6}$ , the sliding frictional moment  $M_{sl} = \mu_{sl}G_{sl}$ , the frictional moment of seals  $M_{seal} = K_{s1}d_s^\beta + K_{s2}$  and the frictional moment of drag loss, churning and splashing.  $G_{rr}$ ,  $G_{sl}$ ,  $\beta$  and  $K_{s1}$  are variables that depend on the bearing,  $v$  is the kinematic viscosity of the lubricant at the operating temperature,  $n$  is the rotational speed,  $\mu_{sl}$  is the sliding friction coefficient and it depends on the oil,  $K_{s2}$  is a variable that depends on the seal type of the bearing and  $d_s$  is the seal counterface. This model, developed by the bearing manufactured, allows the simulation of each kind of operating conditions providing extremely accurate results.

Figures 8–13 show both the experimental and the computation results for the different oil levels and as a function of temperature and rotational speed.

Figure 9: Experimental and computation results for  $L = 0$  mm.Figure 10: Experimental and computation results for  $L = -20$  mm.Figure 11: Experimental and computation results for  $L = 20$  mm.

Due to the high computational time needed for the solution of the numerical models, not all the experimentally tested conditions have been computed with the CFD analysis.

The first three diagrams show that the churning power loss decrease with temperature and with lubricant level. The decrease rate with temperature is very high for low temperatures and

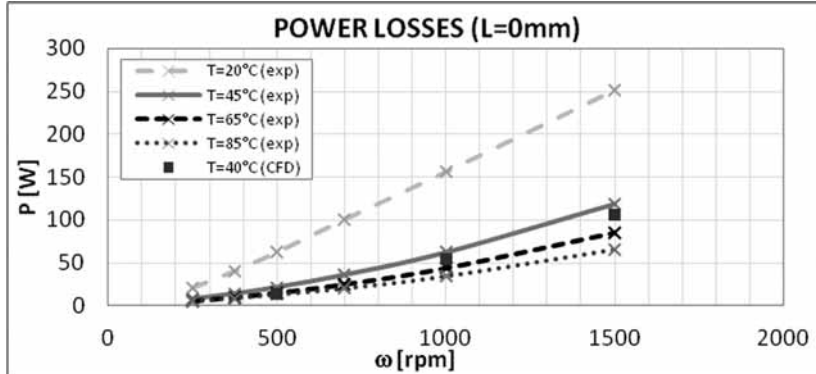


Figure 12: Experimental and computation results for  $L = 0$  mm.

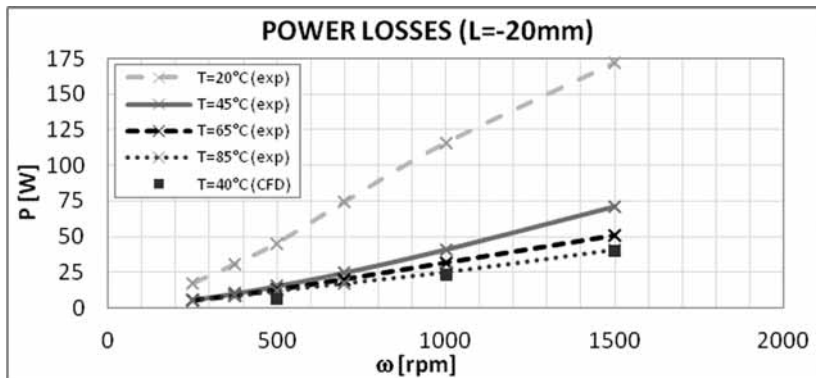


Figure 13: Experimental and computation results for  $L = -20$  mm.

decreases for high temperatures. The relation between churning loss and temperature is well described by a piecewise-linear function. This fact points out the importance to optimize the working temperature to find a good compromise between efficiency and the typical problems that arise with temperature.

The figures show also that the losses increase with lubricant level. The last tree graphs show that the power loss increases with rotational speed. The increase is more than linear.

On the graphs the computational results are also reported. The numerical results are in good agreement with the measured ones. The difference are quite significant only for the lowest lubricant level. In this conditions, in fact, the absolute value of the loss is very low and also little errors in the calculations or in the measurements produce a high relative error.

Figures 14–16 show the results in terms of normalized units. On the X axis, there is the number of Reynolds, defined as  $Re = \frac{\rho VD}{\mu}$ , where  $\rho$  is the density of the lubricant,  $V$  is the characteristic speed ( $V = r\omega$ , where  $r$  is the distance between the gearbox axis and the axis of the planets),  $D$  is the external diameter of the planets and  $\mu$  the dynamic viscosity of the oil.

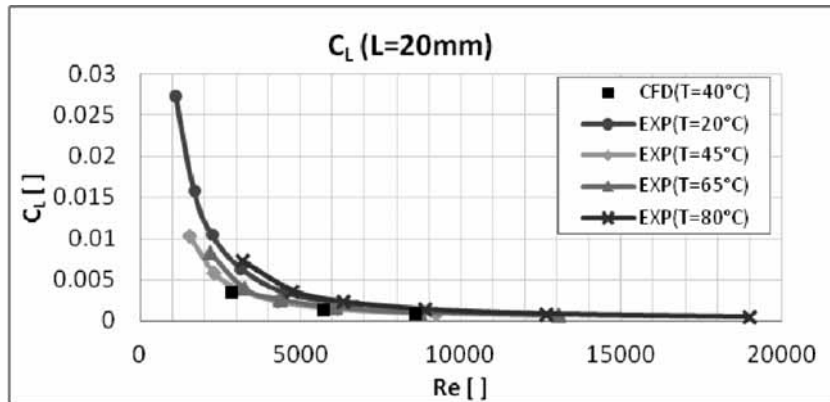


Figure 14: Experimental and computation results for  $L = 20$  mm.

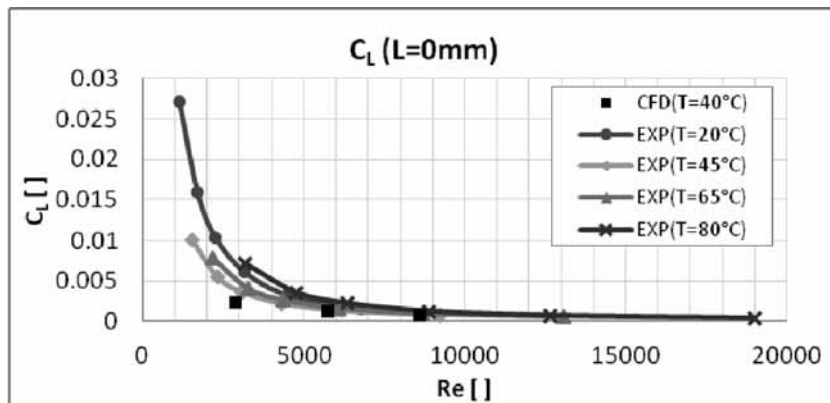


Figure 15: Experimental and computation results for  $L = 0$  mm.

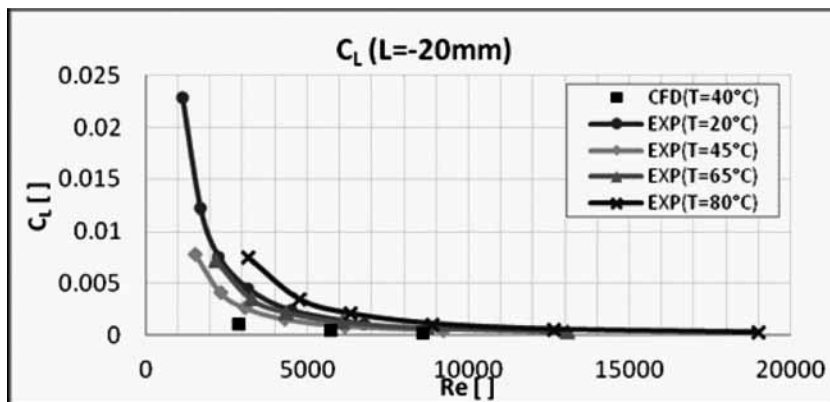


Figure 16: Experimental and computation results for  $L = -20$  mm.

On the  $Y$  axis, there is the loss coefficient defined as  $C_L = \frac{C}{\frac{1}{2} \rho V^2 S}$ , where  $C$  is the resistant torque on the planet carrier shaft  $S$  and is the characteristic surface  $S = n \cdot D \cdot b$  in which  $n$  is the number of planets and  $b$  their thickness.

From these diagrams it is possible to make a comparison between the measured data at 45°C and the computated ones at 40°C. The graphs show a very good agreement between the measured and the computational results except for the lowest lubricant level. A reason for this mismatch can be found in the uncertainty of the measure of the oil level in the experiments. The static level of this quantity, in fact, was measured by means of a transparent pipe at the beginning of each test. An equal absolute error becomes significant if the mean measured value is low. Furthermore, in the simulation, the system adopted to measure the oil level was not modelled. The volume of this transparent pipe was not negligible and maybe its presence has affected the measure.

## 7 CONCLUSIONS

As reliable models to predict the churning loss of the planetary gears are still not available, a computational fluid dynamic analysis has been performed. A multiphase VOF model has been applied to predict the additional source of churning loss typical of epicycloid gear reducers. The input for the model are the geometry of the reducer and the operating conditions.

The results of the model are well supported by the experiments (except for extremely low temperatures).

Applying this model to different operating conditions and performing some experiments, the influence of three different parameters on this kind of losses has been studied. The analysed parameters are the lubricant level, the lubricant temperature and the rotational speed of the planet carrier.

The results show that the losses increase, as expected, with static lubricant level and rotational speed and decrease with the temperature. The decrease rate of the power loss with the temperature is very high for low temperature and decreases with the temperature growth. The relation between churning loss and temperature is well described by a piecewise-linear function.

The increase rate of the losses with the rotational speed is, in turn, more than linear.

Future development are seen in the investigation of other influence parameters like the oil type and the geometry of the reducer.

## REFERENCES

- [1] *General Catalogue SKF* — SKF Group, December 2006.
- [2] Niemann, G. & Winter, H., *Maschinenelemente – Band 2: Getriebe Allgemein, Zahnradgetriebe – Grundlagen, Stirnradgetriebe – 2. Auflage*, Springer: Berlin, 2003.
- [3] ISO/TR 14179–1 and –2.
- [4] Patankar, S.V., *Numerical Heat Transfer and Fluid Flow*, Taylor & Francis: USA, 1980.
- [5] Concli, F., Gorla, C., Arigoni, R., Cognigni, E. & Musolesi, M., *Planetary Speed Reducers: Efficiency, Backlash, Stiffness*, International Conference on Gears, Munich, 2010.
- [6] Concli, F., Gorla, C., Arigoni, R. & Musolesi, M., *Riduttori di precisione a gioco ridotto ed alta efficienza*, Organi di trasmissione – febbraio 2011, Tecniche Nuove: Milano, 2011.

- [7] Csoban, A. & Kozma, M., Influence of the oil churning, the bearing and the tooth friction losses on the efficiency of planetary gears. *Journal of Mechanical Engineering*, **56(4)**, pp. 231–238, 2010.
- [8] Concli, F. & Gorla, C., Computational and experimental analysis of the churning power losses in an industrial planetary speed reducer. *Advances in Fluid Mechanics 2012 Conference Proceedings*, 2012.
- [9] Concli, F. & Gorla, C., Churning power losses in planetary speed reducer: computational-experimental analysis. *EngineSOFT International Conference 2012 Conference Proceedings*, 2011.
- [10] Concli, F. & Gorla, C., *Analisi numerica e sperimentale delle perdite per sbattimento in un riduttore epicicloidale industriale*, Organi di trasmissione – dicembre 2011, Tecniche Nuove: Milano, 2011.
- [11] Versteeg, H.K., Malalasekera, W., *An Introduction to Computational Fluid Dynamics – The Finite Volume Method*, Longman Group: London, 1995.
- [12] Comini, G., *Fondamenti di termofluidodinamica computazionale*, SGEditoriali: Padova, 2004.